The infrared dielectric tensor and axial dispersion in caesium L-malate monohydrate

2007 J. Phys.: Condens. Matter 19 176225

(http://iopscience.iop.org/0953-8984/19/17/176225)

IOP PUBLISHING JOURNAL OF PHYSICS: CONDENSED MATTER

J. Phys.: Condens. Matter **19** (2007) 176225 (12pp) doi:10.1088/0953-8984/19/17/176225

The infrared dielectric tensor and axial dispersion in caesium L-malate monohydrate

J L Ribeiro, L G Vieira, I Tarroso Gomes, D Isakov, E de Matos Gomes and M Belsley

Centro de Física, Universidade do Minho, Campus de Gualtar, 4710-057 Braga, Portugal

Received 3 January 2007, in final form 8 February 2007
Published 10 April 2007
Online at stacks.iop.org/JPhysCM/19/176225

Abstract

Caesium hydrogen L-malate monohydrate ($CsH(C_4H_4O_5)\cdot H_2O$) is a novel coordination compound of L-malic acid and caesium that crystallizes into a monoclinic structure and shows promising properties for application as a piezoelectric, pyroelectric and electro-optic material. In the present work we use polarized infrared reflectivity measurements to investigate the dielectric tensor of the material in the spectral range of 40–4000 cm^{-1}. The use of a three-polarization technique allows us to obtain from the reflectivity data the parameters that characterize the B phonons with wavevectors varying in the plane perpendicular to the monoclinic axis. Consequently, we are able to monitor the frequency dependence of the orientation of the principal dielectric axes in this plane. Using these results we can evaluate the role of polar phonons in the low frequency dielectric response, characterize the dielectric tensor in the terahertz frequency range and describe the axial optical and dielectric dispersion over the frequency range investigated.

(Some figures in this article are in colour only in the electronic version)

1. Introduction

The search for new organic dielectric materials is increasingly motivated by their potential for practical applications in electronics and optics. There exists, in fact, a largely unrealized possibility of using organic molecules with very high electronic polarizability and/or appreciable dipolar moments to fabricate crystalline lattices with exceptional polar properties. Unfortunately, due to lack of control over the positional and orientational degrees of freedom of the molecular units there are quite often serious difficulties in crystallizing the compounds or in inducing the adequate non-centrosymmetric structures that are necessary to obtain desirable properties, such as pyroelectricity, ferroelectricity and second-harmonic generation.

One possible way of circumventing these problems for tailoring appropriate crystalline structures is to exploit the inherent flexibility of hydrogen bonds. Hydrogen tartrate anions, for example, have been used to build 2D anionic layers [1, 2] that allow the synthesis of materials with useful nonlinear optical properties like imidazolium hydrogen tartrate [3].

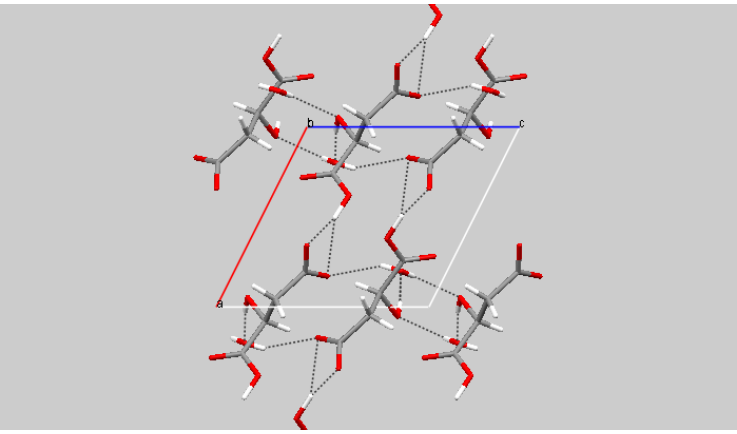

Figure 1. The crystal structure of CsLM projected on the crystallographic *ac* plane. The hydrogen malate molecules form head to tail chains oriented along the *a* axis. These chains are interconnected by hydrogen bonds via the water molecules that align along the *c* axis. The caesium atoms have been removed for clarity.

Also, adequate supramolecular assembly of non-polar conjugated molecules has produced ferroelectric materials with low molecular weight, large spontaneous polarization and high dielectric constants, as in the case of the co-crystals of phenazine and chloranilic acid [4]. In this respect, L-malic acid is an interesting compound to explore. The presence of complementary hydrogen-bonding sites means that this optically active molecule tends to form 2D layers by bonding adjacent ions into chains (through head to tail O–H $\cdots$ O interactions) that are cross-linked via the hydroxyl group [5]. This tendency seems to be preserved in the presence of a variety of counterions and because of its specific molecular chirality its compounds tend to crystallize into non-centrosymmetric structures described by space groups containing only rotation or/and screw axes [6]. Interestingly, the presence of both enantiomers during crystal growth may give rise to glide planes, mirror planes or inversion centres between the two enantiomers, thus producing centrosymmetric lattices on average. This effect, observed in several racemic salts of this acid [7], can be avoided by using molecules of a given chirality.

For these reasons, we have searched for new mixed organic–inorganic systems based on L-malic acid. Caesium hydrogen L-malate monohydrate (hereafter referred to as CsLM: $CsH(C_4H_4O_5)\cdot H_2O$) is one example of a novel coordination compound in this family of materials that display promising characteristics for technological applications. The synthesis and structure of single crystals of CsLM has been recently reported [7, 8]. The crystals have a monoclinic unit cell with two molecular units, lattice parameters $a = 7.4464$ Å, $b = 7.4920$ Å, $c = 7.8555$ Å, $\alpha = \gamma = 90°$, $\beta = 116.73°$ and space group $P2_1$ (see figure 1). The structure consists of irregular eight-coordinated Cs–O polyhedra forming zigzag chains directed along the *b* axis. These polyhedral chains are then inter-connected by hydrogen malate molecules that form head to tail chains directly along the *a* axis. In these chains, the carboxyl group COOH of each anion is hydrogen bonded to both the oxygen atoms of the carboxylate group COO^-. This forms a relatively rigid structure that deforms the torsion angle of the C1–C2–C3–C4 of the hydrogen malate molecules. In addition, the water molecules are aligned along the *c* axis via hydrogen bonds, thus forming layers of malate anions oriented parallel to the *ac* plane. Such consecutive layers are hydrogen bonded to the oxygen atoms of the water molecules. Notably, there is a large net dipolar moment formed by the Cs cations and the COO^- group (38D per unit cell) [8]. This sizable dipole is directed nearly parallel to the crystallographic *b* axis.

The non-centrosymmetric structure and the important value of the dipolar moment per unit cell obtained from x-ray data led us to investigate in more detail the dielectric properties of CsLM. We have looked for the existence of ferroelectricity and characterized its pyroelectric, piezoelectric and electro-optic response. This investigation, which will be reported in a separate article, indicated that CsLM has in fact promising characteristics for use as a piezoelectric, pyroelectric and electro-optical crystal. In this work we explore the technique of polarized reflectivity to characterize the lattice dynamics and assess the dielectric and optical axial dispersion of CsLM in the infrared frequency range. The results reported allow us to evaluate the role of polar phonons in the low frequency dielectric response, characterize the dielectric tensor in the terahertz range and describe the axial optical and dielectric dispersion.

Several devices for the emerging field of terahertz spectroscopy, imaging and ultrahigh bandwidth electro-optic signal processing require novel materials and adequate methods to characterize, in a given material, the relationship between polaritonic dispersion and crystal optics [9, 10]. In the case of crystals with symmetry lower than orthorhombic, as is the case for CsLM, the necessary characterization of that relationship is not easy to obtain because the principal dielectric axes are not fixed by symmetry and may vary with frequency [11]. In addition, the straightforward adaptations of the methods used in the visible range to observe the dispersion of dielectric and optical axes are not very effective in the infrared and microwave ranges because of the difficulties raised by the strong lattice absorption [12, 13]. Light scattering experiments have been used to try to characterize the dielectric tensor in the infrared, as in the case of monoclinic $LiSO_4{\cdot}H_2O$ [14], but these studies are rare, especially in the case of complex organic compounds with several overlapping phonon resonances. Polarized infrared reflectivity may represent a useful alternative and the study described below has been in part motivated by the idea of exploring this possibility.

2. Experimental details

Caesium hydrogen L-malate monohydrate was synthesized from a water solution of analytical grade reagent, caesium hydroxide and L-malic acid, in a 1:1 molar ratio. This solution was stirred at 60 °C for several hours and allowed to cool down to room temperature. Single monoclinic crystals of CsLM (space group $P2_1$) were then grown from a saturated water solution of the compound by using an isothermal solvent evaporation technique. Crystals of good optical quality, stable in air and with large faces parallel to the twofold axis were obtained after several weeks (typical dimensions: $a \times b \times c \approx 5 \times 30 \times 15$ mm^3). These crystals were oriented and parallelepiped samples were cut with major faces oriented parallel or perpendicular to the monoclinic axis. The samples were ground and finely polished using Stuers's synthetic short nap (MD-Nap) with diamond grain size of 15 μm.

The polarized infrared reflectivity spectra were measured at room temperature and near normal incidence with a Bruker IFS 66 V spectrometer. The average angle of incidence was roughly 11°. A set of different light sources, beam splitters, polarizers and detectors were used to cover the frequency range 40–4000 cm^{-1}. In the middle infrared range (500–4000 cm^{-1}) we used a Globar source, a KBr beam splitter, a KRS-5 polarizer and a DTGS:KBr detector. The far infrared region was studied with an Hg lamp, a 6μ-M8 Mylar beam splitter, a polyethylene polarizer and a DTGS-PE detector. The polarizers were mounted in the optical path of the incident beam. The polarizer rotation was performed using a computer controlled mechanical device. The references for calibration of the absolute reflectivity were registered with a gold mirror for each of the polarization directions employed.

The orientation of the principal dielectric axes in the *ac* plane was independently measured at the near infrared frequency of 9398 cm^{-1} ($\lambda = 1064$ nm) with a standard cross-polarizers

method. The three principal refractive indices of the crystal were also measured at the same frequency using a Mach–Zehnder interferometer [15, 16].

3. The method of dispersion analysis

Methods of analysis of the reflectivity data such as conventional dispersive analysis or Kramers–Kronig inversion may be used when the dielectric function and the reflectivity coefficient can be considered as scalars. This condition is satisfied when the polarization of the incident light is directed along a principal axis of the dielectric tensor over the measured spectral range. In the case of crystals with orthorhombic or higher symmetry one can always meet such a requirement because the principal dielectric axes are fixed by symmetry. However, in the case of monoclinic and triclinic crystals, the direction of a principal dielectric axis may depend on the frequency (dispersion of dielectric axes) [11]. In fact, in the case of a monoclinic system like CsLM, only the twofold axis corresponds to symmetry imposed dielectric axis (Y axis). The other two axes lie in the ac plane; their orientations can vary with frequency and are not known *a priori*.

For the case of incident light polarized along the twofold axis we have evaluated the dielectric function $\varepsilon_b(\omega)$ both by Kramers–Kronig inversion and by fitting the factorized form of the dielectric function [17],

$$\varepsilon_Y(\omega) = \varepsilon_Y^{\infty} \prod_{j=1}^{N} \frac{\Omega_{j\mathrm{LO}}^2 - \omega^2 - \mathrm{i}\omega\Gamma_{j\mathrm{LO}}}{\Omega_{j\mathrm{TO}}^2 - \omega^2 - \mathrm{i}\omega\Gamma_{j\mathrm{TO}}}, \tag{1}$$

to the reflectivity spectra at normal incidence, via

$$R_Y(\omega) = |r_Y|^2 = \left| \frac{\sqrt{\varepsilon_Y(\omega)} - 1}{\sqrt{\varepsilon_Y(\omega)} + 1} \right|^2. \tag{2}$$

In equation (1), $\Omega_{j\mathrm{TO(LO)}}$ and $\Gamma_{j\mathrm{TO(LO)}}$ represent the frequency and damping coefficients of the jth transverse (longitudinal) optical mode, while ε_Y^{∞} is the electronic contribution to the dielectric constant. From the fitting, the oscillator strength $\Delta\varepsilon_j$ of each mode can be evaluated as

$$\Delta\varepsilon_j = \frac{\varepsilon_Y^{\infty}}{\Omega_{j\mathrm{TO}}^2} \frac{\prod_{k=1}^{N} \left(\Omega_{k\mathrm{LO}}^2 - \Omega_{j\mathrm{TO}}^2\right)}{\prod_{k\neq j}^{N} \left(\Omega_{k\mathrm{TO}}^2 - \Omega_{j\mathrm{TO}}^2\right)}. \tag{3}$$

Due to the difficulties raised by the complexity of the spectra and by the many overlapping reflectivity bands, during the initial fitting stage we have imposed the condition of equal damping coefficients for longitudinal and transverse optical modes ($\Gamma_{j\mathrm{LO}} = \Gamma_{j\mathrm{TO}}$). Under such a condition, the factorized form (1) corresponds to the conventional sum of polar Lorentz oscillators. We subsequently relaxed this condition to allow for different longitudinal and transverse damping factors. However, we have checked that $\sum_j (\Gamma_{j\mathrm{TO}} - \Gamma_{j\mathrm{LO}}) \approx 0$ in order to verify that the imaginary part of the fitted dielectric function decays more rapidly than with ω^{-1} as $\omega \to \infty$ and that the absorption vanishes at high frequencies [17, 18]. The value of $\varepsilon_Y^{\infty} = 2.26$ was established from the measurement of the refractive index $n_2 = 1.50(\vec{E} \parallel \vec{b})$ at the frequency of 9398 cm^{-1}.

In the case of incident light polarized on the ac plane, we have used a three-polarization measurement technique [19, 20]. Accordingly, we measured the reflectivity at near normal incidence in the ac plane with light polarized along the directions $\theta = 45°$ (axis X), $\theta = 90°$ and $\theta = 135°$ (axis Z), θ representing the angle between the electric field of the incident radiation and the c crystallographic axis. In addition as a control, we have measured a fourth polarization corresponding to $\theta = 0°$.

Following [20] and using the XZ orthogonal system of coordinates, we considered the 2D symmetric tensor $\hat{\varepsilon}_{XZ}(\omega)$ as[1]:

$$\hat{\varepsilon}_{XZ}(\omega) = \hat{\varepsilon}^{\infty}_{XZ} + \sum_i \frac{\Delta\varepsilon_i \Omega^2_{\mathrm{TO},i}}{\Omega^2_{\mathrm{TO},i} - \omega^2 - \mathrm{i}\Gamma_i\omega} \begin{bmatrix} \cos^2\alpha_i & \sin\alpha_i\cos\alpha_i \\ \sin\alpha_i\cos\alpha_i & \sin^2\alpha_i \end{bmatrix}. \tag{4}$$

Here, $\Omega_{\mathrm{TO},j}$, $\Delta\varepsilon_i$, Γ_i represent respectively the transverse optical frequency, the dielectric strength and the damping coefficient of the ith mode; α_i denotes the angle between the dipolar moment of the ith mode and the X axis; $\hat{\varepsilon}^{\infty}_{XZ}$ represents the 2D dielectric tensor at high frequencies. The components of this tensor in the chosen basis were estimated from the measurement of the principal refractive indexes in the ac plane at 9398 cm^{-1} ($\lambda = 1064$ nm). The two orthogonal principal axes were found to be oriented 99° (axis 1) and 9° (axis 3) relative to the crystallographic c axis and the corresponding experimental indices were found to be $n_1 = 1.54$ and $n_3 = 1.49$ ($\varepsilon_1 = 2.37$ and $\varepsilon_3 = 2.22$) respectively. Consequently, the components of $\hat{\varepsilon}^{\infty}_{XZ}$ in the experimental reference frame XYZ were obtained by an appropriate rotation ($\varepsilon^{\infty}_{XX} = 2.318$, $\varepsilon^{\infty}_{ZZ} = 2.271$ and $\varepsilon^{\infty}_{XZ} = -0.071$).

In a similar manner to using equation (2), the complex reflectivity tensor $\hat{r}_{XZ}(\omega)$ was obtained from $\hat{\varepsilon}_{XZ}(\omega)$ as

$$\hat{r}_{XZ}(\omega) = \left[\hat{1} - \sqrt{\hat{\varepsilon}_{XZ}(\omega)}\right]\left[\hat{1} + \sqrt{\hat{\varepsilon}_{XZ}(\omega)}\right]^{-1}, \tag{5}$$

where $\hat{1}$ represents the unity tensor[2].

The dependence of the reflectivity on the frequency for each of the chosen directions of polarization for the incident light ($\hat{e} = \frac{\vec{E}}{|\vec{E}|}$) was obtained via $R_{XZ}(\omega, \hat{e}) = |\hat{r}_{XZ}(\omega)\hat{e}|^2$ as

$$\begin{aligned} R_{\theta=45^\circ}(\omega) &= |r_{XX}(\omega)|^2 + |r_{XZ}(\omega)|^2 \\ R_{\theta=90^\circ}(\omega) &= (|r_{XX}(\omega) + r_{XZ}(\omega)|^2 + |r_{XZ}(\omega) + r_{ZZ}(\omega)|^2)/2 \\ R_{\theta=135^\circ}(\omega) &= |r_{ZZ}(\omega)|^2 + |r_{XZ}(\omega)|^2. \end{aligned} \tag{6}$$

The phonon parameters in equation (4) were obtained by simultaneously fitting the formulae given above to the three experimental reflectivity spectra. In the fitting process, we have used a Levenberg–Marquardt algorithm that iteratively varied the parameters until the weighted mean square difference between the experimental and calculated spectra was minimized.

As is shown explicitly in [21], any three reflectivity spectra measured with incident light polarized along different directions on the ZX plane allow us to generate the spectrum for any other polarization direction on this plane. For example, $R_{\theta=0^\circ}(\omega)$ can be expressed as $R_{\theta=0^\circ}(\omega) = R_{\theta=45^\circ}(\omega) + R_{\theta=135^\circ}(\omega) - R_{\theta=90^\circ}(\omega)$. For consistency, we have measured the fourth spectrum ($R_{\theta=0^\circ}(\omega)$) and checked that this relation was verified within the experimental accuracy.

The knowledge of the parameters fitted to equation (4), to recover the measured reflectivity spectra, allowed us to follow the frequency dependence of $\hat{\varepsilon}_{XZ}(\omega)$. In particular, we were able to calculate the frequency dependence of the two sets of orthogonal eigenvectors of the real and imaginary parts of this tensor lying in the monoclinic plane.

Explicitly, up to a multiple of 90°, the angle ϕ made by one of these axes with the crystallographic c axis is expressed for each frequency as

[1] Since there is no applied magnetic field, the dielectric tensor must be symmetric if we neglect the effect of optical activity.

[2] The square root of the matrix means that the matrix $\hat{\varepsilon}_{ac}(\omega)$ is calculated by reducing it to a diagonal form by a proper rotation, taking the square root of the diagonal elements and rotating it back to the initial basis.

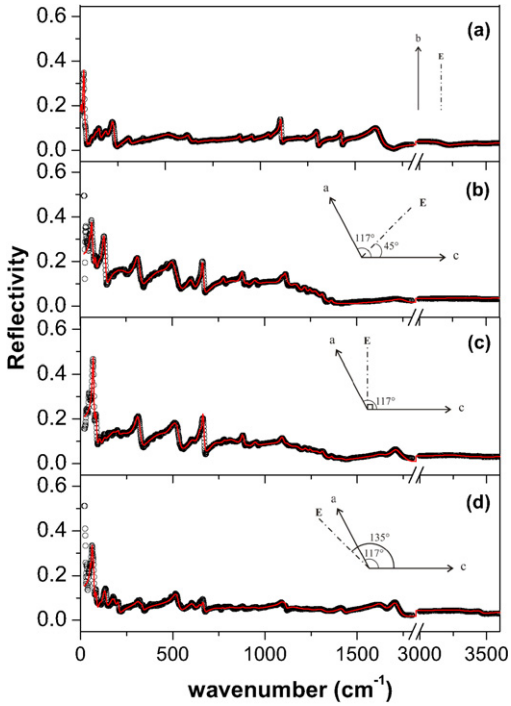

Figure 2. Experimental reflectivity spectra measured at room temperature (circles) with incident light polarized along the $\vec{b}$ axis (a) and in the ac plane ((b)–(d)). The spectra (b)–(d) correspond to incident light polarized along directions forming angles of $\frac{\pi}{4}$ (b), $\frac{\pi}{2}$ (c) and $\frac{3\pi}{4}$ (d) relative to the crystallographic c axis (see the insets). The lines shown correspond to fits of the data to the model functions described in the text.

$$\phi_{\mathrm{R\,(I)}} = \frac{1}{2}\arctan\left(\frac{2\varepsilon_{XZ}^{\mathrm{R\,(I)}}(\omega)}{\varepsilon_{XX}^{\mathrm{R\,(I)}}(\omega) - \varepsilon_{ZZ}^{\mathrm{R\,(I)}}(\omega)}\right) + \frac{\pi}{4}, \tag{7}$$

where R and I specify the real and the imaginary components of $\hat{\varepsilon}_{XZ}(\omega)$, respectively.

In principle, the knowledge of the frequency dependence of the dielectric tensor allows us to obtain the location of the optical axes at any given frequency. For a biaxial crystal with permittivity eigenvalues $\varepsilon_1 > \varepsilon_2 > \varepsilon_3$, the optical axes are located in the plane defined by the principal dielectric axes n_1 and n_3 and form angles of $\pm\beta$ with respect to the axis n_1 such that [11]

$$\tan(\beta) = \pm\sqrt{\frac{\varepsilon_3}{\varepsilon_1}\frac{\varepsilon_2 - \varepsilon_1}{\varepsilon_3 - \varepsilon_2}}. \tag{8}$$

4. Experimental results and discussion

As referred to above, CsLM crystallizes into a monoclinic structure with space group $P2_1$ and two molecular units per unit cell. Factor group analysis indicates that there exists a set of $53\mathrm{A} \oplus 52\mathrm{B}$ vibrational modes active in the infrared.

The A and B modes are detected for incident light polarized as $\vec{E} \parallel \vec{b}$ and $\vec{E} \perp \vec{b}$, respectively. Figure 2 shows the reflectivity spectra measured with these two geometries. Figure 2(a) corresponds to the polarization $\vec{E} \parallel \vec{b}$ and figures 2(b), (c) to polarizations $\vec{E} \perp \vec{b}$

with polarization directions oriented 135°, 90° and 45° with respect to the crystallographic c axis.

In the higher frequency region (above 1300 cm^{-1}), the vibrational spectra exhibit bands characteristic of the L-malate group, such as those related to the ν(OH) vibrations, ν(CH) and $\nu(CH_2)$ vibrations, symmetric and asymmetric stretching vibrations of the carboxylic group, together with CH deformation bands and coupled vibrations of COOH groups. In the range of 900–1300 cm^{-1}, one can observe bands related to the ν(CO), ν(CC) and CH and OH deformation vibrations. In the range 400–900 cm^{-1}, we observe bands related to deformation vibrations of the COO, OH, CH and CH_2 groups. Tentative assignments of some bands are given in table 1 with the help of references [22–25]. The range below 300 cm^{-1} corresponds to the region of the external modes.

The reflectivity spectra were analysed according to the methods outlined in the previous section. Figure 2 shows the experimental data (circles) and the reflectivity curves (lines) corresponding to the best fits obtained from the model functions (1) ($\vec{E} \parallel \vec{b}$) and (6) ($\vec{E} \perp \vec{b}$). In the fitting process we have considered the minimum number of modes necessary to satisfactorily account for the essential features of the experimental spectra. The model parameters obtained for the different reflectivity bands are given in table 1. We have included in the fits 30A ($\vec{E} \parallel \vec{b}$) and 46B ($\vec{E} \perp \vec{b}$) vibrational modes.

Because each reflectivity spectrum contained over 4000 frequency points, the ratio between the number of parameters to be adjusted and the number of experimental points is 3×10^{-2} for the $\vec{E} \parallel \vec{b}$ spectrum and 1.5×10^{-2} for the $\vec{E} \perp \vec{b}$ spectra. From this point of view, the expected confidence in the analysis of the reflectivity of light polarized in the monoclinic plane seems similar to that of the standard analysis of the $\vec{E} \parallel \vec{b}$ reflectivity, as the increasing in the number of adjustable parameters is compensated by the increasing of the number of the data points. In order to assess the order of magnitude of the errors in the adjustment of these parameters, we repeated the fitting several times starting from different initial conditions. We have found that values of the transverse optical frequencies Ω_{TO} and angle α characterizing the orientation of the corresponding electric dipole were typically well reproduced within 5%, while the values of the damping and strength were less stable (±20%).

As is often the case in complex spectra of organic compounds, the number of modes adjusted in both experimental geometries is inferior to the number expected from symmetry analysis. This indicates that some bands may have strengths too faint to be detected or are unresolved because of overlap in frequency with other bands. However, it is apparent that the difference between the number of bands detected and allowed by symmetry is more important for the $\vec{E} \parallel \vec{b}$ geometry (30 and 53, respectively) than for the $\vec{E} \perp \vec{b}$ geometry (46 and 52, respectively). This may be partially due to the peculiarities of the crystal structure. As referred to above, the head to tail chains of hydrogen malate molecules are directed along the a axis and are mainly interconnected by the water molecules that align along the c axis via hydrogen bonds. Therefore, because this geometry corresponds to a sequence of layers of malate anions mainly oriented parallel to the ac plane, one may expect to detect more easily the internal modes of the organic group with incident light polarized in the ac plane. In other words, the dielectric strength of one internal vibrational mode of B symmetry originating from a given chemical bond of the group are likely to be larger than that of the corresponding A symmetry mode.

Another reason for the difference in number of modes detected between the two geometries is that the three angle technique used to analyse the $\vec{E} \perp \vec{b}$ spectra may allow for an enhanced resolution of bands located close together in frequency. In fact, because the analysis is simultaneously made for the three spectra measured with incident light polarized along different directions, two modes very close in frequency but with different polarization angles may be

Table 1. The model parameters corresponding to the best fit of equations (1) and (4) to the reflectivity data, measured for polarizations $\vec{E} \parallel \vec{b}$ and $\vec{E} \perp \vec{b}$, respectively. The last column of the table lists the assignment of some of the reflectivity bands, obtained from the comparison of the experimental spectra with the data taken from [18–21].

$\vec{E} \parallel \vec{b}$					$\vec{E} \perp \vec{b}$				
Ω_{TO} (cm^{-1})	Γ_{TO} (cm^{-1})	Ω_{LO} (cm^{-1})	Γ_{LO} (cm^{-1})	$\Delta\varepsilon$	Ω_{TO} (cm^{-1})	Γ (cm^{-1})	$\Delta\varepsilon$	α (deg)	Assignment
58	8	60	6	0.317	53	4	0.340	−45	
					61	7	0.925	−49	
68	6	74	7	0.721	67	7	1.703	46	
79	13	84	10	0.223	83	12	0.501	51	
94	9	95	9	0.038					
					106	19	0.219	60	Lattice modes
115	9	116	9	0.022					
					127	14	1.005	−62	
136	19	137	20	0.044					
152	11	154	12	0.077					
191	18	193	17	0.073	182	32	0.217	−14	
					205	14	0.063	−4	
222	21	233	20	0.226	239	108	0.760	82	
312	22	315	22	0.041	312	28	0.375	67	C-COOH in plane bending
					336	16	0.033	−28	
386	7	387	7	0.001					$\delta(COH)_{rock}$, δCC, δCOO
					444	119	0.447	78	δCH, δCC
					499	53	0.289	91	
523	87	531	102	0.072	522	35	0.138	21	
					602	43	0.096	111	ECHB
623	27	627	29	0.024	614	39	0.043	20	
					649	20	0.041	47	νCC, δOH, δCH_2
665	12	666	12	0.002	662	11	0.059	61	νCC, δOH, δCH_2
764	17	765	17	0.001	740	69	0.054	55	ECHB
					780	15	0.013	107	δCH_2
					822	115	0.171	241	
895	9	896	10	0.004	878	17	0.025	74	γCH, ν(C–C)
					906	10	0.002	95	γCH, ν(C–C)
					943	62	0.009	156	
958	15	960	15	0.005	947	25	0.011	67	νCC, δCO
1050	12	1051	12	0.004	1052	364	0.646	79	γCH, νCC
1084	92	1085	110	0.008	1092	27	0.016	51	ν(C–C); ν (C–O)
1108	9	1112	10	0.015	1111	17	0.019	−50	δCH_{2sciss}
					1167	48	0.018	107	
					1177	160	0.071	−3	
1208	16	1209	16	0.001	1216	26	0.009	99	$\delta(CH_3)_{twist}$; δCH_{2scis}
1236	15	1237.0	15	0.002	1244	42	0.004	192	$\delta CH_{2wag.}$
					1245	18	0.004	91	
					1273	48	0.017	101	
1301	16	1305	12	0.015	1310	20	0.005	75	$\nu CO + \delta OH$
					1311	69	0.019	−4	$\nu CO + \delta OH$
1352	151	1356	157	0.014	1362	13	0.002	69	δ (CH) of CHOH
1428	9	1430	8	0.007	1422	33	0.010	−13	δCH_2
					1566	51	0.004	−4	
1612	69	1639	67	0.074	1632	67	0.035	−7	νCO_{asym}
					1645	182	0.002	−48	
1693	46	1694	39	0.001	1709	54	0.040	3	$\nu C = O$ dimeric COOH
					1745	98	0.030	58	$\nu C = O$ dimeric COOH
3198	168	3205	142	0.009					νOH hydr. bond COOH
3350	204	3351	193	0.001	3320	228	0.016	17	νOH water
3462	119	3466	116	0.005	3455	59	0.005	−16	νOH of CHOH

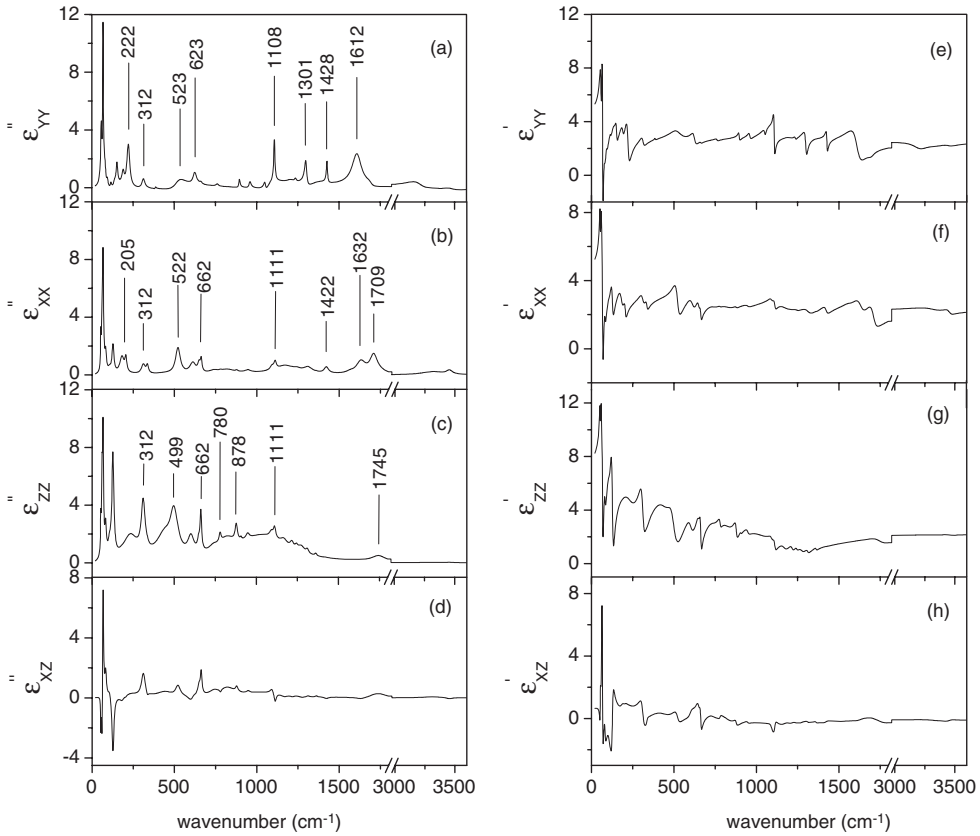

Figure 3. The dispersion of the components of the complex dielectric tensor in the XYZ reference frame. The imaginary and real parts of these components are separately shown in (a)–(d) and (e)–(h), respectively. The vibration modes that give rise to pronounced dispersion effects are identified in (a)–(c).

well discriminated. This spatial resolution of the polarization of the modes does not exist in conventional dispersion analysis.

The values of the parameters listed in table 1 allow us to recover the components of the complex dielectric tensor via equations (1) and (4). Figures 3(a)–(h) show the real and imaginary parts of these components as a function of frequency. As can be seen, the dispersion of the dielectric tensor markedly reflects the resonances related to the polar phonon modes. We have identified in the figure the transverse optical frequencies of the modes that give rise to pronounced variations of the dielectric tensor.

The knowledge of the frequency dependence of the dielectric tensor allows us to analyse the axial dielectric dispersion in the ac plane. The principal dielectric axes in this plane are not fixed by symmetry and are not related to any specific crystallographic direction. The rotation of the dielectric ellipse can be characterized by the angle Φ between one of its principal axes and the c crystallographic direction. However, the real and imaginary components of the dielectric tensor cannot in general be simultaneously diagonalized over a single system of real coordinates. That is, in crystals of monoclinic or triclinic symmetry, the permittivity $\hat{\varepsilon}'$ and the optical conductivity $\hat{\sigma} = \frac{\omega\hat{\varepsilon}''}{4\pi}$ tensors do not in general share common sets of eigenvectors. Therefore, figure 4 displays the frequency dependence of the angles Φ_R and

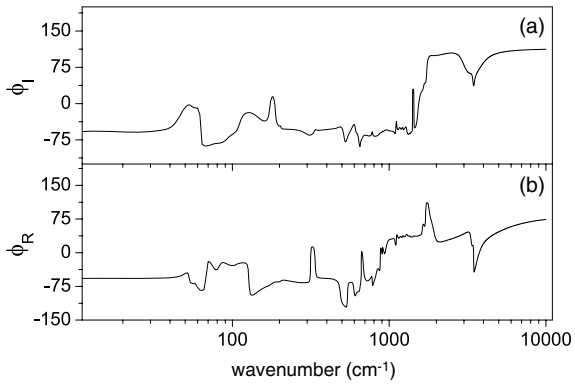

Figure 4. Frequency dependence of the angles Φ_R and Φ_I characterizing the orientation of the principal dielectric axes of the permittivity (a) and dielectric loss (b) in the *ac* plane. In both cases, the angles shown correspond to the dielectric axis n_1 and are measured relative to the crystallographic *c* axis. The orientation of axis n_3 is defined by the corresponding angles $\Phi_{R,I} + \frac{\pi}{2}$.

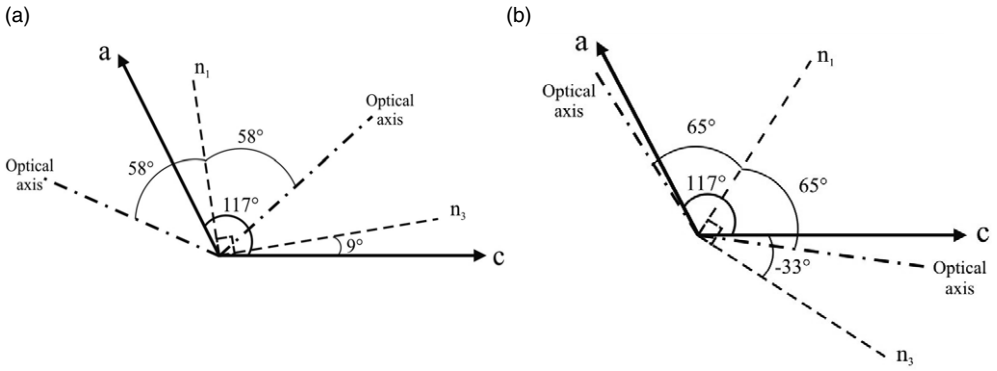

Figure 5. Axial dispersion in CsLM: orientation of the optical axes and principal dielectric axes of the permittivity in the *ac* plane for the frequencies of 9398 cm^{-1} (a) and 1 cm^{-1} (b).

Φ_I that, according to (7), define the orientation of the two sets of principal axes with respect to the *c* crystallographic direction.

The effect of axial dielectric dispersion in CsLM is substantial and errors in the determination of phonon parameters would result if the rotation of the principal axes were ignored, for instance, by using the standard methods of dispersion analysis of the reflectivity data. Note that, because in (7) the angle Φ is determined up to a factor of $n\frac{\pi}{2}$, the curves depicted in figure 4 were obtained by choosing solutions that allow continuity of both Φ and $\frac{d\Phi}{d\omega}$ over the frequency range investigated. We have also taken into account the axial orientation determined experimentally at high frequencies for the permittivity. The parameters obtained also allow us to estimate the components of the dielectric tensor below the frequency range of the phonons. These components characterize the lattice contribution to the static permittivity, i.e., define the static permittivity in the absence of possible relaxational contributions occurring at lower frequencies. At 1 cm^{-1}, the principal values of this tensor are $\varepsilon_1 = 8.15$, $\varepsilon_2 = 5.31$ and $\varepsilon_3 = 4.95$. The principal directions corresponding to ε_1 and ε_3 are located in the *ac* plane approximately oriented at $-33°$ and $57°$ with respect to the *c* axis (see figure 5). The

orientations of the optical axes on the *ac* plane, as estimated from (8), are shown in figure 5 and compared with those observed at optical frequencies.

5. Conclusion

The study of the dielectric and optical properties of monoclinic and triclinic crystals is severely complicated by the fact that there is lack of an appropriate orthogonal coordinate system to use in the description of such properties. The geometric dispersion effects of the optical and dielectric axes that are at the origin of such difficulties can be observed and mapped from polarized infrared reflectivity measurements. The use of a three-polarization technique first proposed in [15] allowed us to characterize the lattice dynamics of monoclinic CsLM and, in particular, observe the directional dispersion of oblique B phonons. The full characterization of the dielectric tensor thus obtained provides us with the means to calculate the frequency dependence of the optical and dielectric ellipsoids in the infrared range.

The reliability of the method depends essentially on the accuracy of the fits of the model dielectric functions to the reflectivity data. This point is particularly relevant in the case of organic crystals such as CsLM, where the reflectivity spectra are quite complex. For the spectra measured in the monoclinic plane, the adjustment of $\hat{\varepsilon}^{\infty}_{XZ}$ is critical because it defines a reference frame that affects all the fits. Here, we circumvent this difficulty by using the experimental components of this tensor measured independently by other means. Under these circumstances, the similar ratio between the number of experimental points and the parameters to be adjusted suggests that the quality of fit of these spectra is similar to that obtained from a standard fit of isotropic reflectivity.

References

[1] Aakeroy C B, Hitchcock P B and Seddon K R 1992 *J. Chem. Soc., Chem. Commun.* 553
[2] Zyss J, Pecaut J, Levy J P and Masse R 1993 *Acta Crystallogr.* B **49** 334
[3] Aakeroy C B and Hitchcock P B 1993 *J. Mater. Chem.* **3** 1129
[4] Horiuchi S, Ishii F, Kumai R, Okimoto Y, Tachibana H, Nagaosa N and Tokura Y 2005 *Nat. Mater.* **4** 143
[5] Aakeroy C B and Nieuwenhuyzen M 1996 *Chem. Mater.* **8** 1229
[6] Fleck M, Tillmanns E, Bohaty L and Held P 2004 *Z. Kristallogr.* **219** 101
[7] Fleck M, Tillmanns E and Bohaty L 2001 *Z. Kristallogr.* **216** 633
[8] de Matos Gomes E, Gonçalves C F, Belsley M S, Ferreira F, Costa M M R, Rodrigues V H and Criado A 2005 *Proc. SPIE* **5912** 59120D
[9] Ferguson B and Cheng Zhang X 2002 *Nat. Mater.* **1** 26
[10] Stoyanov N S, Ward D W, Feurer T and Nelson K A 2002 *Nat. Mater.* **1** 95
[11] Born M and Wolf E 1959 *Principles of Optics* (Cambridge: Cambridge University Press)
[12] Claus R 1978 *Phys. Status Solidi* b **88** 683
[13] Claus R and Borstel G 1978 *Phys. Status Solidi* b **88** K123
[14] Lang W and Claus R 1982 *Phys. Rev.* B **26** 7119
[15] McKee D J, Nicholls J F and Ruddock H 1995 *Eur. J. Phys.* **16** 127
[16] Dixit V K, Vanishri S, Bhat H L, de Matos Gomes E, Belsley M, Santinha C, Arunmozhi G, Venkataramanan V, Proença F and Criado A 2003 *J. Cryst. Growth* **253** 460
[17] Berreman D W and Unterwald F C 1968 *Phys. Rev.* **174** 791
[18] Ribeiro J L and Vieira L G 2003 *Eur. Phys. J.* B **36** 21
[19] Belousov M V and Pavinich V F 1978 *Opt. Spectrosc.* **45** 771
Pavinich V F and Belousov M V 1978 *Opt. Spectrosc.* **45** 881
Pavinich V F and Bochtarev V A 1988 *Opt. Spectrosc.* **65** 640
[20] Kuz′menko A B, van der Marel D, van Bentum P J M, Tishchenko E A, Presura C and Bush A A 2001 *Phys. Rev.* B **63** 094303
[21] Kuz′menko A B, Tishchenko E A and Orlov V G 1996 *J. Phys.: Condens. Matter* **8** 6199

[22] Pretsch E, Clerc T, Seibl J and Simon W 1983 *Spectral Data for Structure Determination of Organic Compounds* (Berlin: Springer)
[23] Baranska H, Kuduk-Jaworska J, Szostak R and Romaniewska A 2003 *J. Raman Spectrosc.* **34** 68
[24] Baranska H, Kuduk-Jaworska J and Waszkiewicz K J 2000 *J. Mol. Struct.* **550/551** 307
[25] Wolfs I and Desseyn H O 1996 *Appl. Spectrosc.* **50** 1000